Numerical simulation of axisymmetric drop formation using a coupled level set and volume of fluid method

I. Chakraborty [1], M. Rubio-Rubio[1], A. Sevilla[1], J.M. Gordillo[2]

[1]*Departamento de Ingenieria Termica y de Fluidos, Universidad Carlos III de Madrid, Spain*

[2]*Area de Mecanica de Fluidos, Departamento de Ingenieria Aeroespacial y Mecanica de Fluidos, Universidad de Sevilla,Spain*

[*]Email addresses for correspondence: indracster@gmail.com and asevilla@ing.uc3m.es.

ABSTRACT

Numerical simulations have been carried out to examine the axisymmetric formation of drops of Newtonian liquid injected from a vertical orifice under constant flow conditions into ambient air. The numerical simulation was performed by solving axisymmetric Navier–Stokes equations with a coupled level-set and volume-of-fluid (CLSVOF) method. In this work, the dynamics of the formation of drops are investigated over a range of the Ohnesorge number Oh=0.01, 0.023 and 0.13, and the Bond number Bo=0.33, 0.5 and 2.205, as the Weber number We increases. The different responses of drop formation such as period-1 dripping with (P1S) or without satellite drops (P1), complex dripping (CD) and jetting (J) are discussed. The different responses of drop formation were identified quantitatively from the time history of growing length of drop at the orifice. The transition of different responses is shown on the map which exhibits the variation of limiting length of drop at breakup or the volume of the detached primary drop with We while keeping Oh and Bo fixed. The numerical investigation of liquid jet formation in terms of the evolution of growing length of jet under different computational grid sizes was discussed. It is proposed that the stable liquid jet formation can be found as the mesh size decreases. The accuracy of the present computed results is assessed by comparisons with the previous investigations. Furthermore, it is shown that at high Bo=2.205, low Oh=0.023 and We=0.0177, the system exhibits period-2 with satellite drop (P2S) response which was not reported before in literature.

Keywords: Numerical simulation, CLSVOF, Drop formation, Dripping, Jetting, Transition

1. Introduction

Drop formation is of great interest for various applications such as spraying and ink-jet printing technologies (Shield et al., 1987), separation and extraction processes (Heideger and Wright,

1986), and among others (Basaran, 2002). On the other hand, the study of drop formation has been a topic of scientific research interest due to the richness of underlying physics (Eggers, 1997). Most commonly, drops are produced by injecting a liquid through a nozzle or an orifice into ambient air. Many investigations of the basic case of drop formation were reviewed by Eggers (1997), Clift et al. (1978), Kumar and Kuloor (1970) and Eggers and Villermaux (2008). The subject of drop formation from capillary tube under the influence of gravity has been extensively investigated both experimentally (Wilson, 1988; Peregrine and Shoker, 1990; Zhang and Basaran, 1995; Henderson et al., 1997; Clanet and Lasheras, 1999; Ambravaneswaran et al., 2000; Ambravaneswaran et al., 2004; Subramani et al., 2006) and numerically (Eggers and Dupont, 1994; Ambravaneswaran et al., 2000; Ambravaneswaran et al., 2002; Ambravaneswaran et al., 2004; Yildirim et al., 2005; Subramani et al., 2006; Schulkes, 1994; Zhang and Stone, 1997; Wilkes et al., 1999; Zhang, 1999; Gueyffier et al., 1999; Chen et al., 2002; Che et al., 2011; Pan and Suga, 2006; Delteil et al., 2011) and among others. In this paper, we present a computational study of drop formation by the injection of a liquid from a vertical orifice into the ambient air under constant flow conditions.

There are two responses of drop formation discussed in most previous investigations. These are the dripping and jetting. At low and moderate liquid flow rates at the orifice, drops are formed close to the orifice which is known as dripping. At high flow rates, the drops are created far downstream from the orifice exit and a long column of continuous liquid jet formation can be observed known as jetting. At very small flow rates, the primary drops and much smaller secondary drops (satellites) are formed periodically in time (Peregrine and Shoker, 1990; Zhang and Basaran , 1995; Henderson et al., 1997; Eggers and Dupont, 1994; Ambravaneswaran et al., 2000; Ambravaneswaran et al., 2002; Ambravaneswaran et al., 2004; Yildirim et al., 2005; Subramani et al., 2006; Schulkes, 1994; Zhang and Stone, 1997; Wilkes et al., 1999; Zhang, 1999; Gueyffier et al., 1999). This regime is known as period-1 dripping with satellites (hereafter referred to as P1S). When the liquid flow rate is increased to a critical value, above which the primary drops without satellite drops formation can be observed known as period-1 dripping (Clanet and Lasheras, 1999; Ambravaneswaran et al., 2000; Ambravaneswaran et al., 2002; Ambravaneswaran et al., 2004; Yildirim et al., 2005; Subramani et al., 2006; Schulkes, 1994; Zhang and Stone, 1997; Zhang, 1999) (hereafter referred to as P1). In P1S and P1 responses, equal sized primary drops in succession with constant frequency can be observed. As the flow rate is increased further, the period-1 dripping gives way to complex dripping (Clanet and Lasheras, 1999; Ambravaneswaran et al., 2000; Ambravaneswaran et al., 2004; Subramani et al., 2006) (hereafter referred to as CD) where nonlinear dynamics of drop formation (period-2, period-3,

period-4 and chaotic responses) are observed. The period-2, period-3 and period-4 responses (hereafter referred to as P2, P3 and P4) are characterized by regularly repeating two, three and four distinct drop volumes and formation periods, respectively. On the other hand, the dynamics of drop formation can not be predicted with time when the system response is chaotic. At sufficiently high flow rates, the drops are created from the ends of a long column of continuous jet due to the well known Rayleigh instability (Rayleigh, 1879), which is known as jetting (Clanet and Lasheras, 1999; Ambravaneswaran et al., 2004; Subramani et al., 2006; Pan and Suga, 2006; Delteil et al., 2011) (hereafter referred to as J). In dripping, the dynamics of drop formation is governed by the interplay of inertial, viscous, gravity and surface tension forces. However, at sufficiently low flow rates, the volume of detached drop is determined by the balance of surface tension and gravity forces and the drop volume is independent of liquid flow rates (Kumar and Kuloor, 1970; Wilson, 1988; Peregrine and Shoker, 1990; Zhang and Basaran , 1995; Henderson et al., 1997; Clanet and Lasheras, 1999; Yildirim et al., 2005; Schulkes, 1994; Zhang and Stone, 1997; Wilkes et al., 1999; Zhang, 1999; Che et al., 2011). This response is also known as quasi-static response.

According to Wilson, (1988) and Zhang and Basaran (1995), there are two main stages of the drop formation process in dripping, namely the expansion stage and the collapse stage. During the expansion (first) stage, the volume of the drop grows slowly and the detaching forces are weak compared with attaching forces. This stage ends with equilibrium of forces. When the equilibrium of forces is lost the collapse (second) stage starts. During the collapse (second) stage, the detaching forces dominate over the attaching forces. In this stage, the drop is attached at the orifice through neck formation. At the end of this stage, the neck is pinched off and the drop is detached from the orifice. The prediction of the growth and detachment of drop formed from an orifice using 1D slender jet approximations to the Navier-Stokes equations was investigated by Eggers and Dupont(1994). This model was successfully applied to study the dynamics responses (Ambravaneswaran et al., 2000; Ambravaneswaran et al., 2004; Subramani et al., 2006) of P1S, P1, CD and J, and the transition from dripping to jetting (Ambravaneswaran et al., 2004; Subramani et al., 2006). Aside from experimental and numerical investigations based on 1D slender jet approximations, few studies have been reported using full Navier-Stokes equations (Schulkes, 1994; Zhang and Stone, 1997; Wilkes et al., 1999; Zhang, 1999; Gueyffier et al., 1999; Chen et al., 2002; Che et al., 2011; Pan and Suga, 2006; Delteil et al., 2011) on the problem of liquid drop formation into air. Numerical solutions of axisymmetric Navier-Stokes equations with boundary integral method of potential flow (Schulkes, 1994) and Stokes flow (Zhang and Stone, 1997), finite-element method (Wilkes et al., 1999; Chen et al., 2002) and volume-of-fluid method

(Zhang, 1999; Gueyffier et al., 1999) were successfully compared with experimental results. However, they only studied the dynamics of drop formation from a vertical capillary tube under the condition of very small liquid flow rates. Che et al. (2011) studied the growth and breakup of a pendant drop from a capillary using level-set method by solving three-dimensional Navier-Stokes equations. Pan and Suga (2006) investigated the formation of laminar liquid jets into the quiescent air using three-dimensional Navier-Stokes equations. The dynamics of the evolving interface was captured by the level-set method. To the best of the authors' knowledge, numerical studies to investigate the nonlinear dynamics of drop formation into the ambient air using full Navier-Stokes system are still lacking in the literature, a fact which motivated our present study. For this purpose, we have used an in-house interface capturing code based on a coupled level-set and volume-of-fluid (CLSVOF) method (Chakraborty et al., 2009; Chakraborty et al., 2011; Chakraborty et al., 2013) governed by three-dimensional but axisymmetric Navier-Stokes equations for the simulations of two-phase flows. Chakraborty et al.(2009) and Chakraborty et al.(2011) studied the dynamics of bubble formation from an orifice submerged in the quiescent liquid over a wide range of gas flow rate regimes.

Our objective in this work is to elucidate the effects of Weber number (liquid flow rate at the orifice) on the dynamics of drop formation process into air when Bo=0.5 and Oh=0.01 given by Ambravaneswaran et al.(2004), Bo=0.33 and Oh=0.13 given by Subramani et al.(2006), and Bo=2.205 and Oh=0.02. We focus our studies on the growth history of drop in terms of growing length at the orifice, the volume of the detached primary drops and the limiting lengths measured from the orifice to their tips at the moment of breakup. We study the dripping, jetting and the transition of different responses.

2. Formulation of the problem

2.1 Problem description

Complete numerical simulation of the drop formation process was performed in an axisymmetric coordinate (r,z) as shown in Fig.1. It is convenient to use a cylindrical coordinate system (r,z,θ), where r is the radial coordinate, z is the axial coordinate measured in the direction of gravity g and θ is the azimuthal coordinate. The origin of the coordinate system (r,z,θ) is placed at the centre of the orifice. In this paper, the dynamics are assumed to be axisymmetric and the problem is independent of the azimuthal coordinate θ. A Newtonian liquid of density ρ_l and viscosity μ_l is injected at a constant flow rate Q through a single orifice of radius R_o into still air of density ρ_a and viscosity μ_a as shown in Fig.1. We assume t air and the liquid filling the drop to be

incompressible with isothermal conditions. The surface tension σ of the liquid-air interface is spatially uniform and constant in time. In this paper, the drop base is assumed to be pinned with the orifice and the effect of contact angle is not considered.

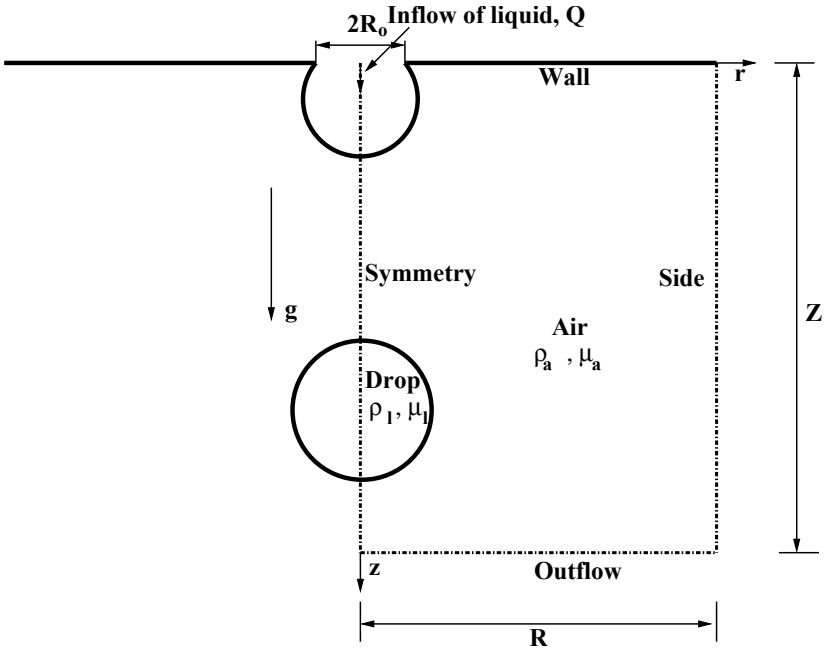

Fig. 1. Schematic of axisymmetric formation of drop from a vertical orifice and computational domain.

2.2. Governing equations and dimensionless groups

In this study, the liquid and ambient gas phases are modeled as single fluid with variable physical properties taking into account the influence of surface tension at the interface. Both phases are immiscible and incompressible fluids. This single fluid takes the properties of the liquid within the drop and those of air within t. It is assumed that the flow in each phase is axisymmetric. The problem is governed by the single set of the governing equations which are the continuity equation as

$$\nabla.\vec{V} = 0 \tag{1}$$

and momentum equation as

$$\rho(\tilde{\alpha})\left(\frac{\partial \vec{V}}{\partial t} + \vec{V}.\nabla\vec{V}\right) = -\nabla p + \rho(\tilde{\alpha})\vec{g} + \nabla.\left[\mu(\tilde{\alpha})\left(\nabla\vec{V} + \left(\nabla\vec{V}\right)^T\right)\right] + \sigma\kappa\nabla\tilde{\alpha} \tag{2}$$

Here, $\vec{V} = (u, v)$ is the velocity vector where u and v stand for radial and axial components of the velocity vector, respectively. p is the pressure, $\vec{g} = (0, g)$ is the gravitational acceleration and t is the time. The influence of surface tension σ is incorporated into the momentum equation

following the continuum surface force (CSF) model of Brackbill et al. (1992). Here, $\tilde{\alpha}$ is the smoothed void fraction field, which is defined using a Heaviside function (Chakraborty et al., 2013; Sussman and Puckett, 2000), $H_\varepsilon(\phi)$, as

$$\tilde{\alpha} = H_\varepsilon(\phi) = \begin{cases} 1 & \phi > \varepsilon \\ \frac{1}{2} + \frac{\phi}{2\varepsilon} + \frac{1}{2\pi}\left[\sin\left(\frac{\pi\phi}{\varepsilon}\right)\right] & |\phi| \le \varepsilon \\ 0 & \phi < -\varepsilon \end{cases} \tag{3}$$

where ϕ is the level set function, which is maintained as the signed distance function from the interface. Here, ϕ is zero at the interface and has positive values in the liquid region and negative values in the gas region. Here, 2ε is the interface thickness over which the fluid properties are interpolated. The present simulations were performed using $\varepsilon = 1.5\Delta r$, where Δr is the size of the computational cell as discussed in detail in Chakraborty et al. (2013). The density $\rho(\tilde{\alpha})$ and viscosity $\mu(\tilde{\alpha})$ can be expressed from a Heaviside function $H_\varepsilon(\phi)$ as

$$\rho(\tilde{\alpha}) = \rho_l\tilde{\alpha} + \rho_a(1-\tilde{\alpha}) \tag{4}$$

$$\mu(\tilde{\alpha}) = \mu_l\tilde{\alpha} + \mu_a(1-\tilde{\alpha}) \tag{5}$$

The local curvature κ of the interface is computed as

$$\kappa = -\nabla.\frac{\nabla\phi}{|\nabla\phi|} \tag{6}$$

In the CLSVOF method (Chakraborty et al., 2013; Sussman and Puckett, 2000; Son and Hur, 2002), the advection for the liquid volume fraction α and the level set function ϕ are,

$$\frac{\partial\alpha}{\partial t} + \nabla.\left(\vec{V}\alpha\right) = 0 \tag{7}$$

$$\frac{\partial\phi}{\partial t} + \vec{V}.\nabla\phi = 0 \tag{8}$$

respectively.

The governing equations are cast in dimensionless form by using the orifice radius R_o as length scale, the capillary time $\sqrt{\rho_l R_o^3/\sigma}$ as time scale, the capillary pressure σ/R_o as pressure scale and the capillary velocity $\sqrt{\sigma/\rho_l R_o}$ as velocity scale. The resulting equations are the continuity equation:

$$\nabla.\vec{V}^* = 0 \tag{9}$$

and the modified momentum equation:

$$\rho^*(\tilde{\alpha})\left(\frac{\partial \vec{V}^*}{\partial t^*}+\vec{V}^*.\nabla\left(\vec{V}^*\right)\right)=-\nabla p^*+\rho^*(\tilde{\alpha})\mathrm{Bo}+(\mathrm{Oh})\nabla.\left[\mu^*(\tilde{\alpha})\left(\nabla\vec{V}^*+\left(\nabla\vec{V}^*\right)^T\right)\right]+\kappa^*\nabla\tilde{\alpha} \tag{10}$$

where the variables with * denote the dimensionless variables. In Eq. (10), the density and viscosity of the single fluid continuum are computed by

$$\rho^*(\tilde{\alpha})=\tilde{\alpha}+\eta(1-\tilde{\alpha}) \tag{11}$$

$$\mu^*(\tilde{\alpha})=\tilde{\alpha}+\lambda(1-\tilde{\alpha}) \tag{12}$$

It is observed from Eqs. 10–12 that there are four dimensionless parameters: the Bond number $\mathrm{Bo}=\frac{\rho_l g R_o^2}{\sigma}$ which measures the relative importance of gravity to surface tension forces; the Ohnesorge number $\mathrm{Oh}=\frac{\mu_l}{\sqrt{\rho_l R_o \sigma}}$ which measures the relative importance of the viscous to surface tension forces; the density ratio $\eta=\rho_a/\rho_l$; and the viscosity ratio $\lambda=\mu_a/\mu_l$. Additionally, the fifth dimensionless parameter Weber number $\mathrm{We}=\frac{\rho_l v_{avg}^2 R_o}{\sigma}$,which measures the relative importance of inertial to surface tension forces, arises due to the liquid inflow rate Q at the orifice. Here, the average inflow velocity of liquid at the orifice inlet is $v_{avg}=Q/\pi R_o^2$.

2.3 Numerical method

The numerical technique used in the present study is a coupled level-set and volume-of-fluid (CLSVOF) method (Chakraborty et al., 2013; Sussman and Puckett, 2000; Son and Hur, 2002) for capturing the movement of interface between two immiscible fluids. In this method, the governing equations (1 and 2) are discretized using the explicit finite-difference method on an axisymmetric coordinate with equidistant grid in the radial and axial directions. The convection and the viscous terms are discretized by a second-order ENO method (Son and Hur, 2002) and central differencing, respectively. The discretized equations are solved on a fixed staggered grid with scalars (p, ϕ and α) located at the cell centers and velocity components ($\vec{V}$) at the center of the cell faces using MAC method (Harlow and Welch, 1965). Based on the new velocity field, the level set function ϕ (Osher and Sethian, 1988) (from Eq. (7)) and volume of the fluid fraction α (Hirt and Nichols, 1981) (from Eq. (6)) are determined using a coupled second order operator split scheme as discussed in Chakraborty et al. (2013) and references therein. The evolution of the interface is captured using level-set function ϕ and the mass is conserved using volume-of-the

fluid fraction α due to the evolving interface. The stability of the solution is confirmed by choosing the time step which satisfies CFL, capillary, viscous and gravitational time conditions reported by Chakraborty et al., 2013. A more detailed description of the numerical method are available in Chakraborty et al.(2013).

2.4 Computational Domain and Boundary Conditions

The computational domain for the axisymmetric formation of drops is shown in Fig. 1. Numerical simulations were carried out to find the effect of side and outflow boundaries at low to high Weber numbers. In the present problem, the computational domain with the width at $R = 5R_o$ in radial direction and the height at $Z = 30R_o$ in axial direction were chosen so that the effect of side and outflow boundaries on the drop formation process can be ignored.

The symmetry or slip boundary conditions at the left or right boundaries, no-slip boundary condition at the wall and Neumann boundary condition at the outflow are imposed. At the orifice inlet, a liquid is injected into an ambient air with a parabolic profile of Poiseuille flow (Chakraborty et al., 2009) in z direction. At the orifice inlet, the Reynolds number $\mathrm{Re}_l = \dfrac{\rho_l v_{avg} D_o}{\mu_l}$ based on the liquid properties is deployed according to the laminar pipe flow condition ($\mathrm{Re}_l < 2300$), where D_o is the orifice diameter. The drop is initially assumed to be pinned with a hemisphere of radius equal to the orifice radius. Initially, the gas and the liquid phases are assumed to be quiescent and at uniform pressure.

2.5 Resolution tests and Validation

To ensure grid independence of the solution, first the mesh refinements studies were carried out to examine the effects of grid resolution on the results as shown in Figs. 2 and 3. The grid independence tests were conducted using 25×75, 50×150, 80×240 and 100×300 grid meshes for the time evolution of dimensionless growing drop length $L^*(=L/R_o)$ for four consecutive drops at $\mathrm{Oh} = 0.13$, $\mathrm{Bo} = 0.33$ and $\mathrm{We} = 0.119$ as shown in Fig. 2. Here, the dimensional growing drop length is denoted by L. Figure 2 shows that the drop formation reaches a stable state after first drop detachment. It is observed that the growth history of drop length for 50×150, 80×240 and 100×300 grid meshes are almost identical, while for 25×75 grid mesh yields differences. In addition, the time evolution of drop formation profiles using the same grid meshes is presented in Fig.3. The results of Fig.3 show that the satellite drop is formed for 25×75,

50×150 and 80×240 grid meshes whereas no satellite drop formation can be observed for 100×300 grid mesh. Subramani et al.(2006) experimentally and numerically using 1-d

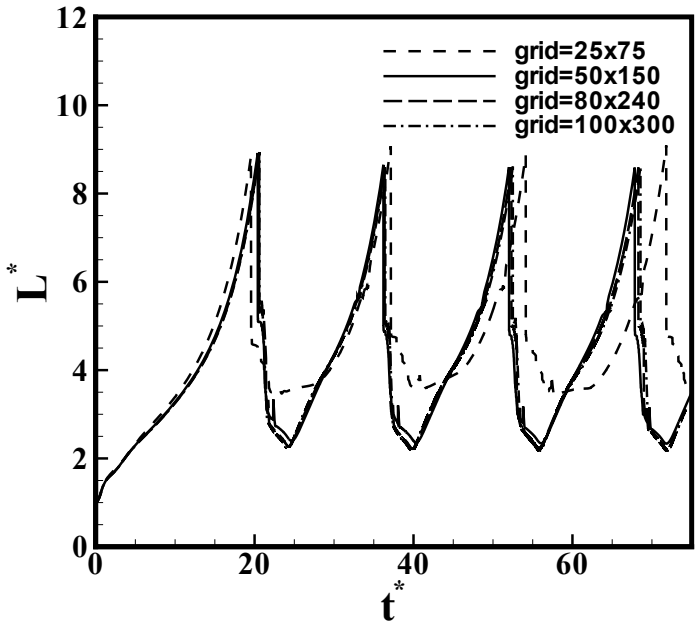

Fig. 2. Effect of mesh size on the temporal variation of dimensionless growing drop length $L^*(=L/R_o)$ for four consecutive drops under the conditions of $Oh=0.13$, $Bo=0.33$, $We=0.119$, $\eta=8.961\times10^{-4}$ and $\lambda=3.165\times10^{-4}$.

approximation found that the dynamics of drop formation process exhibits period-1 without satellite drop (P1) response using the same operating parameters as our present case. Therefore, in this present work, the computations were performed on 100×300 grid mesh without losing the accuracy of the computational results. The values of the dimensionless grid size both in r and z directions and the dimensionless time step are $\Delta r^*=\Delta z^*=0.05$ and $\Delta t^*=10^{-4}$, respectively. However, the corresponding values are used to compute the drop formation process accurately for the dynamics of P1 and CD responses whereas the dynamics of P1S and J were conducted using finer grid size as discussed later.

Figure 4 illustrates the comparison of the drop shape at the incipience of breakup predicted by the present computed result superimposed on the experimental result of Subramani et al.(2006) using the same parameters as in Figs. 2 and 3. Excellent agreement has been found by comparing our computed result (red line) to the experimental result of Subramani et al.(2006). The values of dimensionless limiting length $L_d^*(=L_d/R_o)$ and dimensionless detached primary drop volume

$V_d^*(=V_d/R_o^3)$ of Fig.4 were determined (see also Fig. 2) to make quantitative comparison between our predicted results, and experiment and computation results of Subramani et al.(2006).

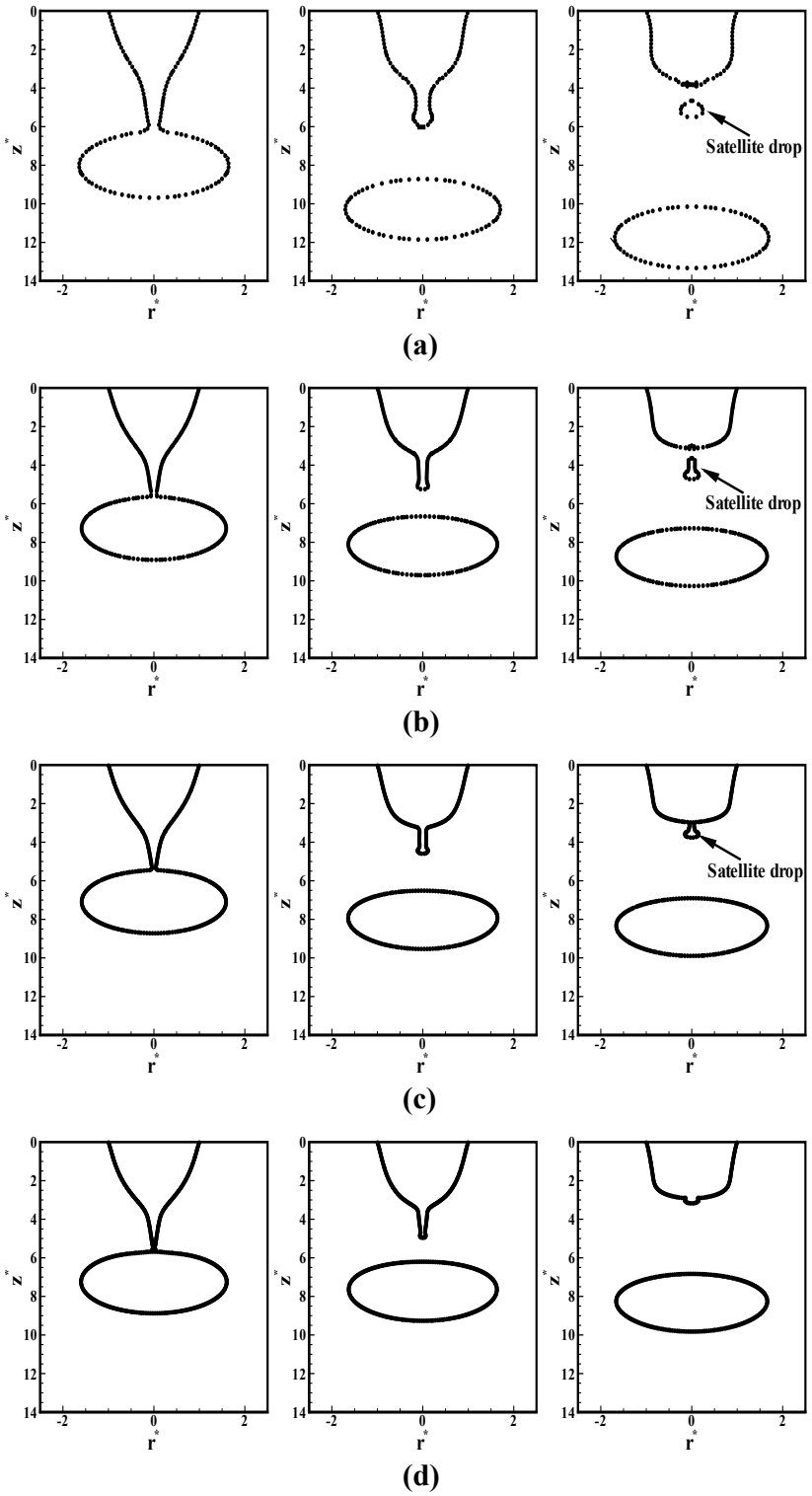

Fig. 3. Effect of mesh size on the drop formation process for the cases of (a) 25×75 grid mesh, (b) 50×150 grid mesh, (c) 80×240 grid mesh and (d) 100×300 grid mesh with the same parameters as in Fig. 2.

Here, the dimensional limiting drop length and dimensional detached primary drop volume are denoted by L_d and V_d, respectively. The experimental and numerical values of L_d^* and V_d^* obtained from the work of Subramani et al.(2006) are $L_{d,ex}^* = 8.6 \pm 0.1$ and $V_{d,ex}^* = 17.4 \pm 0.3$, and $L_{d,1D}^* = 8.65$ and $V_{d,1D}^* = 18.5$, respectively. The corresponding values obtained from our present computation are $L_d^* = 8.62$ and $V_d^* = 17.42$, resulting in errors of about 1% in L_d^* and 1% in V_d^* relative to the experimental values. It is observed that the values of our predicted L_d^* and V_d^* are in reasonably good agreement with the experimental results compared to the computed results obtained from 1D simulation.

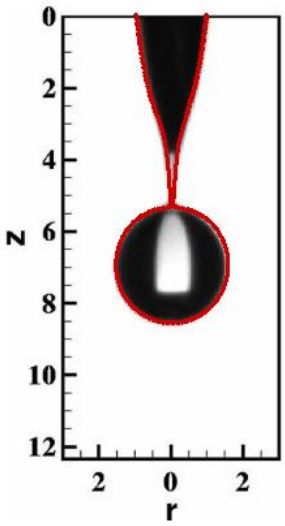

Fig. 4. The comparison of the experiment result of Subramani et al. (2006) with the present computed result (red line) on the incipience of drop breakup using the same parameters as in Figs. 2 and 3.

3. Results and discussions

In this section, the different responses and the transitions of the dynamics of drop formation into an ambient air have been presented. It is our purpose here to find the comparisons between the present computed results and the results obtained in Ambravaneswaran et al.(2004) and Subramani et al.(2006). The values of the governing dimensionless parameters numbers examined for the simulations are listed in Table 1.

Dimensionless Parameter	Range
Bo	$0.33,\ 0.5$ and 2.205
Oh	$0.01, 0.023$ and 0.13
We	$1.8\times10^{-4} - 7.0\times10^{-1}$
η	$8.961\times10^{-4}, 1.0\times10^{-3}\ \ 1.10\times10^{-3}$
λ	$3.165\times10^{-4},\ \ 7.1\times10^{-3},\ 2.20\times10^{-3}$

Table 1: Dimensionless parameters covered for numerical simulations

3.1 Dripping

We report the numerical results of dripping response at $\mathrm{Oh} = 0.01$ and $\mathrm{Bo} = 0.5$ by varying the Weber numbers (liquid flow rates) as shown in Figs. 5 and 6. Figures 5 (a) and 5 (b) show the time evolution of drop formation and growing drop length at the orifice for four consecutive primary drops in P1S response when $\mathrm{We} = 0.019$ and P1 response when $\mathrm{We} = 0.055$, respectively. It is observed from Fig. 5 that all consecutive drops have the same limiting length L_d^*. The results from Fig. 5(a) show that in P1S response a liquid thread is formed and the liquid thread breaks into small satellite drop due to the imbalance force of surface tension. However, as We increases to We=0.055 the satellite drop formation is suppressed and P1 response without satellite drops formation can be observed as shown in Fig. 5(b).

Figure 6 illustrates the time sequence of drop formation and the time history of growing drop length in P2 response when $\mathrm{We} = 0.091$ (see Fig. 6(a)), P3 response when $\mathrm{We} = 0.245$ (see Fig. 6(b)) and P4 response when $\mathrm{We} = 0.333$ (see Fig. 6(c)), respectively. The results from Fig. 6 show that drops of two different L_d^* in P2 response, three different L_d^* in P3 response and four different L_d^* in P4 response are formed successively. Here, satellite drops formation cannot be observed. The similar observations have been found by Ambravaneswaran et al.(2000) and Ambravaneswaran et al.(2004).

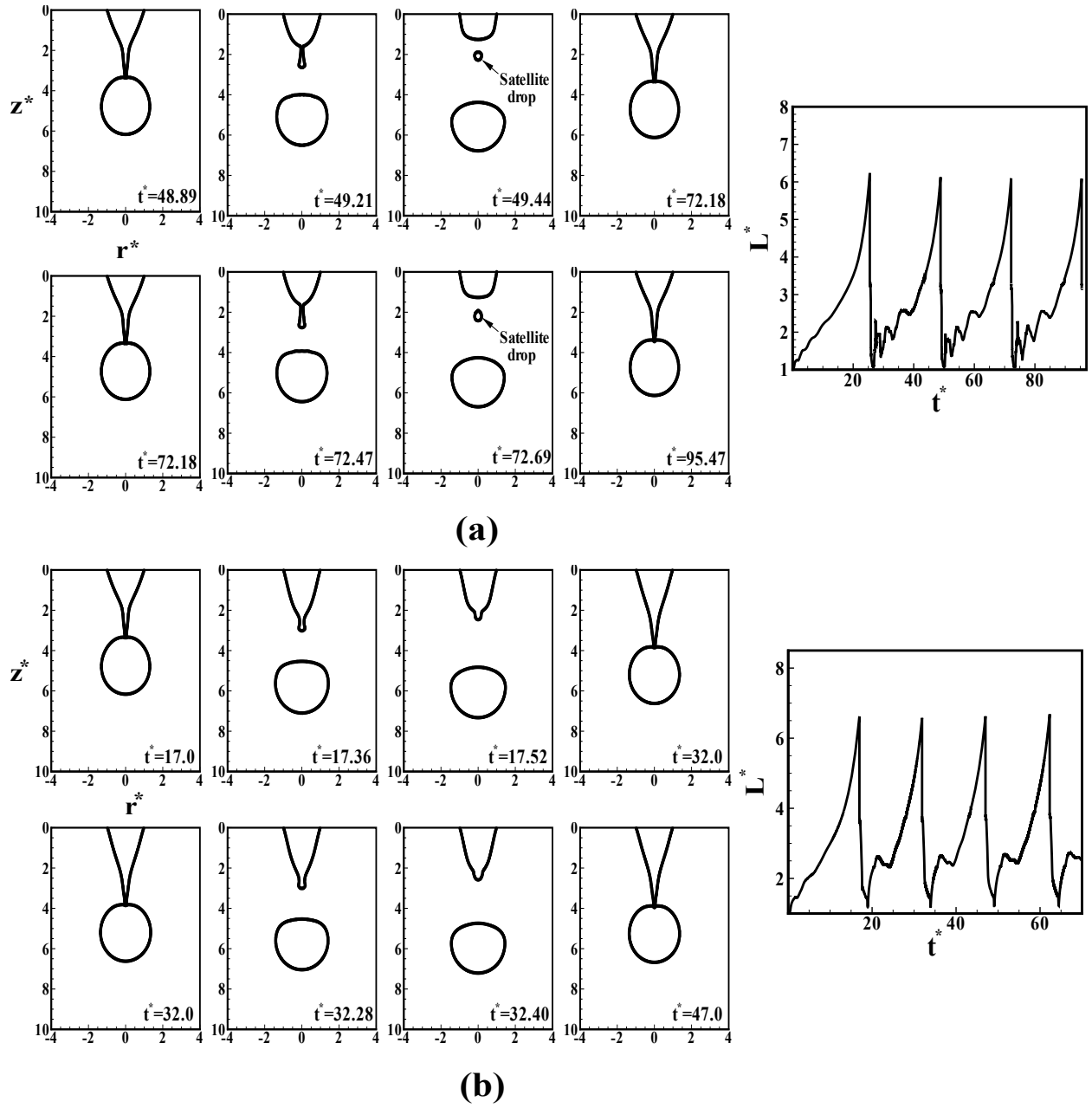

Fig. 5. The computation results of drop formation in P1S and P1 responses at $\mathrm{Oh} = 0.01$, $\mathrm{Bo} = 0.5$, $\eta = 1.0\times10^{-3}$ and $\lambda = 7.1\times10^{-3}$ for the cases of (a) the time evolution of the primary and secondary (satellite) drops formation (left) and the growth history of drop length (right) in PIS response for $\mathrm{We} = 0.019$ and (b) the time evolution of the primary drops formation (left) and the growth history of drop length (right) in P1 response for $\mathrm{We} = 0.055$.

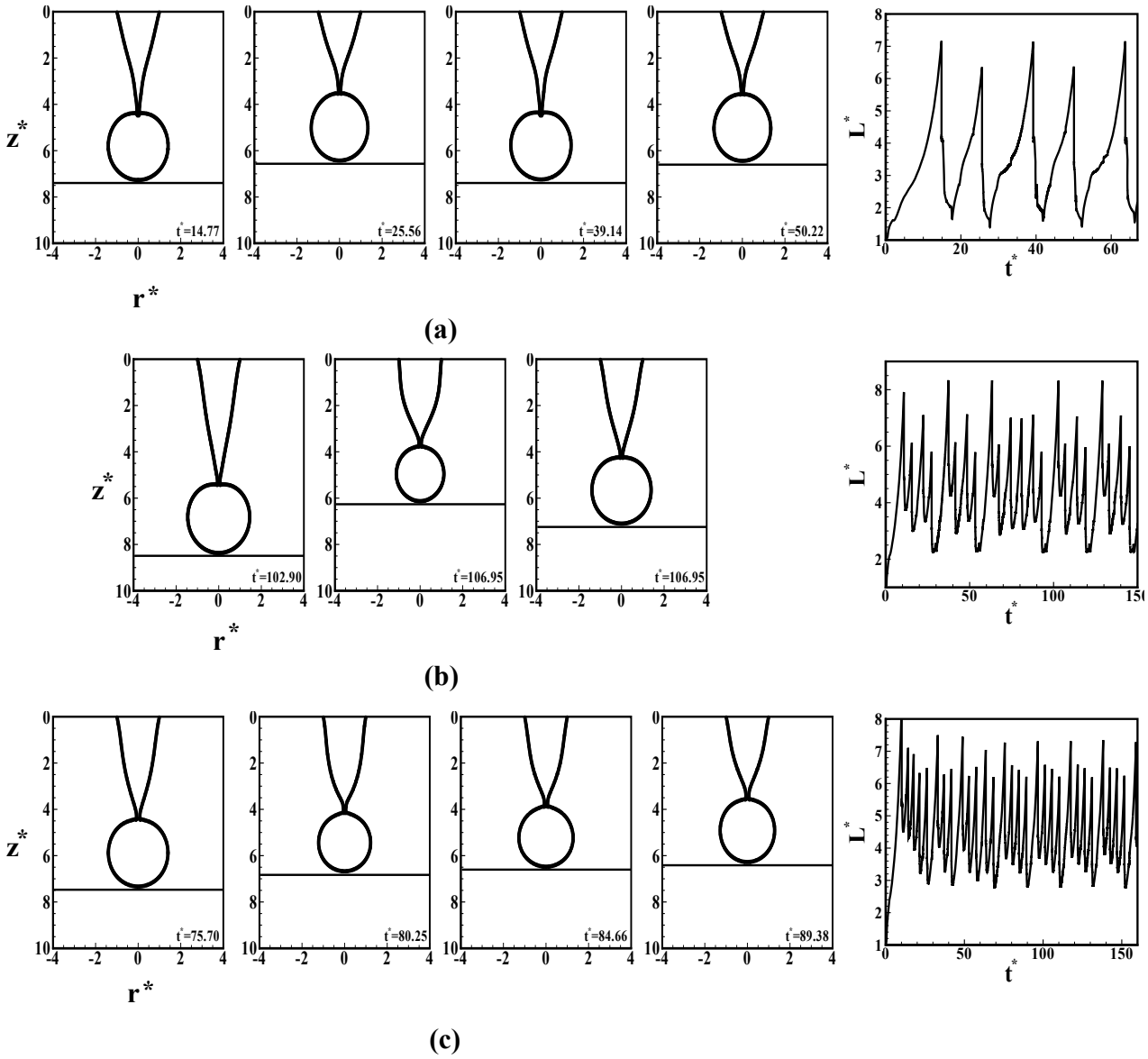

Fig. 6. The computation results of the time instant of the primary drops at the incipience of breakup (left) and the growth history of drop length (right) in P2, P3 and P4 responses at $\mathrm{Oh} = 0.01$, $\mathrm{Bo} = 0.5$, $\eta = 1.0\times10^{-3}$ and $\lambda = 7.1\times10^{-3}$ for (a) $\mathrm{We} = 0.091$ in P2 response, (b) $\mathrm{We} = 0.245$ in P3 response and (b) $\mathrm{We} = 0.333$ in P4 response.

3.2 Jetting

First, we present the results of the growth history of liquid jet length in jetting response at $\mathrm{Oh} = 0.01$ and $\mathrm{Bo} = 0.5$ when $\mathrm{We} = 0.4536$. The liquid jet length variations with time were reported experimentally by Clanet and Lasheras (1999), and numerically by Pan and Suga(2006)

and Delteil et al. (2011). It was observed from their investigations that the limiting length of jet fluctuates with time. Therefore, the discussion of grid convergence study is necessary to achieve

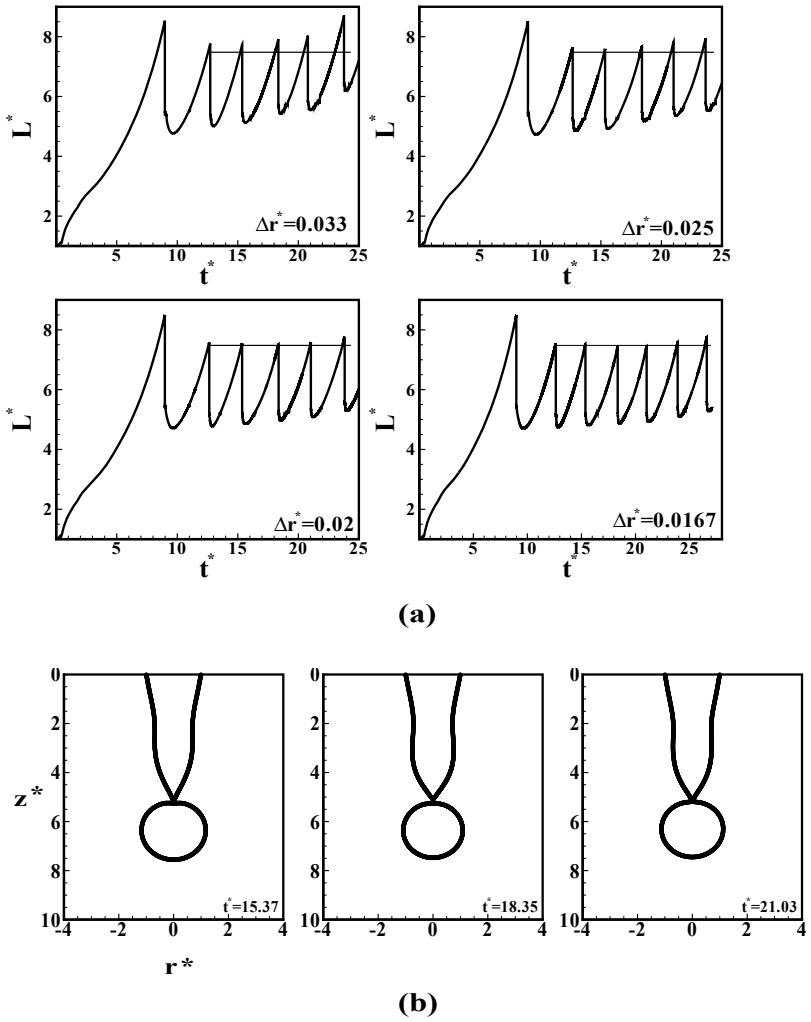

Fig. 7. (a) Computation results of the time evolution of growing drop length in jetting response using different grid mesh sizes and (b) Instantaneous profile of three consecutive drops at the incipience of breakup in jetting response. The pertinent input parameters are $\mathrm{Oh} = 0.01$, $\mathrm{Bo} = 0.5$, $\eta = 1.0\times10^{-3}$, $\lambda = 7.1\times10^{-3}$ and $\mathrm{We} = 0.4596$. The limiting length is approximately $\mathrm{L}_{\mathrm{d}}^{*} \approx 8.00$.

the dynamics of stable liquid jet formation. This study was performed by using four different grid meshes. Figure 7(a) shows the time evolution of growing length of jet for six consecutive drops using grid meshes of 150×450 with $\Delta r^{*} = \Delta z^{*} \approx 0.0333$, 200×600 with $\Delta r^{*} = \Delta z^{*} = 0.025$, 250×750 with $\Delta r^{*} = \Delta z^{*} = 0.02$ and 300×900 with $\Delta r^{*} = \Delta z^{*} \approx 0.0167$. The results from Fig. 7(a) show that the limiting length at breakup of the jet reaches stable as the grid mesh size decreases whereas the limiting length increases with time for coarser grid meshes. It can be

observed that the growing length reaches unstable after four consecutive drops formation for $\Delta r^* = \Delta z^* = 0.02$ and after five consecutive drops formation for $\Delta r^* = \Delta z^* \approx 0.0167$. Therefore, it can be stated that much finer grid mesh would be necessary to achieve the stable jet formation and the time step has to be small enough to obtain the steady jet formation. However, our simulations are unable to find stable liquid jet formation for long time growth history due to limiting computational resources. Finally, time sequence profiles of three consecutive drops at the incipience of breakup in jetting regime are shown in Fig. 7(b) for 300×900 grid mesh with $\Delta r^* = \Delta z^* \approx 0.0167$.

3.3 Transition from Dripping to Jetting

The variation of limiting length L_d^* with Weber number under the conditions of $Oh = 0.01$, $Bo = 0.5$, and $Oh = 0.13$, $Bo = 0.33$ is shown in Figs.8(a) and 8(b), respectively.

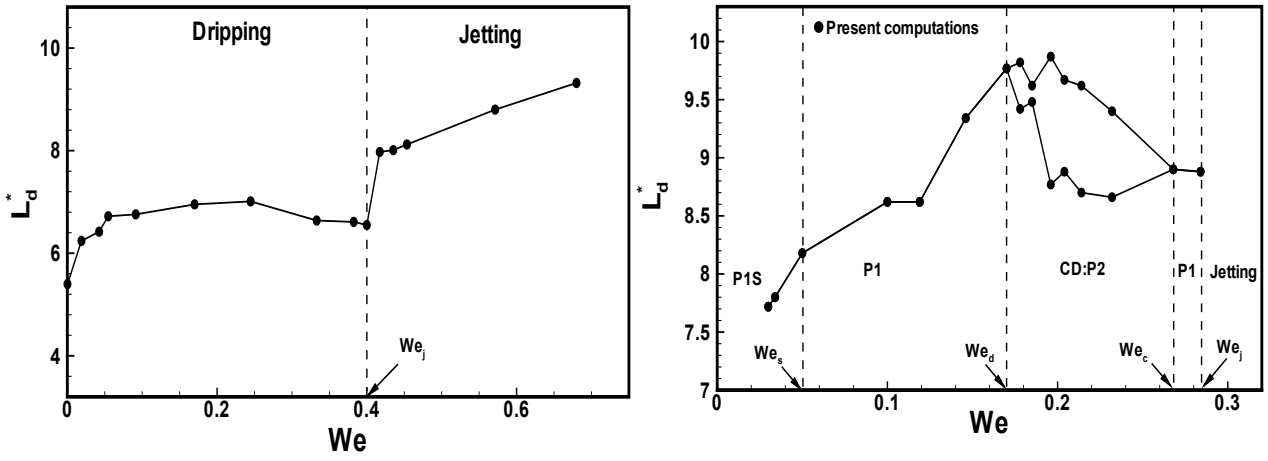

Fig. 8. Computed results that show the variation of limiting length with We for the cases of **(a)** $Oh = 0.01$, $Bo = 0.5$, $\eta = 1.0 \times 10^{-3}$ and $\lambda = 7.1 \times 10^{-3}$. The results also exhibit the transition from dripping to jetting, and (b) $Oh = 0.13, Bo = 0.33$, $\eta = 8.961 \times 10^{-4}$ and $\lambda = 3.165 \times 10^{-4}$. The results also identify the transition of different responses.

Figure 9 reports the bifurcation diagrams, showing the variation of L_d^* with We and V_d^* with We, that compare the present computed results with the results given by Subramani et al.(2006), when $Oh = 0.13$ and $Bo = 0.33$. As shown in Fig. 8(a), the transition point from dripping to jetting occurs at $We = We_j$ beyond which the limiting length suddenly increases to a large value and the

system signals jetting response. Figure 8 (b) known as bifurcation diagram determines the transition points between P1S and P1 which occurs when $We = We_s$ beyond which the satellite drops formation cannot be observed, P1 and complex dripping (CD: P2) denoted by $We = We_d$, and CD:P2 and P1 denoted by $We = We_c$. It is observed that when $We > We_d$ and $We > We_c$, P1

Transition Weber numbers	Experiment	Computation 1-D model	Present work
We_s	------	0.036	0.0425
We_d	0.07	-----	0.0682
We_j	0.48	0.80	0.40

Table 2: Comparison between present results, and experiment (Ambravaneswaran et al., 2004) and computation results based on 1-D model (Ambravaneswaran et al., 2002; Ambravaneswaran et al., 2004) . Here, We_s, We_d and We_j are the critical Weber numbers which signal the transition from P1S to P1, P1 to CD and CD to J, respectively. The pertinent input parameters are $Oh = 0.01$, $Bo = 0.5$, $\eta = 1.0 \times 10^{-3}$ and $\lambda = 7.1 \times 10^{-3}$.

response gives way to CD:P2 and CD:P2 returns again to P1, respectively. As the Weber number is further increased beyond We_c another critical value is found at $We = We_j$ defined the transition from P1 to J, and the system signals to jetting beyond a $We = We_j$. A summary of the comparison of the critical values of Weber numbers is presented in Tables 2 and 3. Figure 8 (a) and Table 2 show that the critical value of Weber number from dripping to jetting occurs at $We_j = 0.4$ whereas the experimental measured value is $We_{j,exp} = 0.48$ (see Fig. 3, in Ambravaneswaran et al.(2004)). The value of critical Weber number based on 1D approximations is $We_{j,1D} = 0.8$ as shown in Fig.2(a) of Ambravaneswaran et al.(2004). It depicts that the present computed We_j is more accurate than that of $We_{j,1D}$. As shown in Fig.9, the predicted results of limiting length, primary drop volume and critical Weber number (see also in Table 3) match quite well with the experimental results compared to the results obtained from 1D simulation of Subramani et al.(2006). However, the predicted critical value of Weber number from P1S to P1 at

$We = We_s$ is higher than the results obtained from experiments (Ambravaneswaran et al., 2004; Subramani et al., 2006) and computations (Ambravaneswaran et al., 2002; Ambravaneswaran et al., 2004; Subramani et al., 2006) as given in Table 2 and 3. The accuracy of the predicted We_s may be found if the grid mesh size is decreased. It is observed from Fig. 9 that for the dimensionless mesh sizes of $\Delta r^* = 0.05$ and $\Delta r^* = 0.025$ the critical values of We_s are 0.05 and 0.045, respectively. When the dimensionless grid size is decreased to $\Delta r^* = 0.0125$ the computation becomes very expensive which is unable to find We_s due to limiting computation resources.

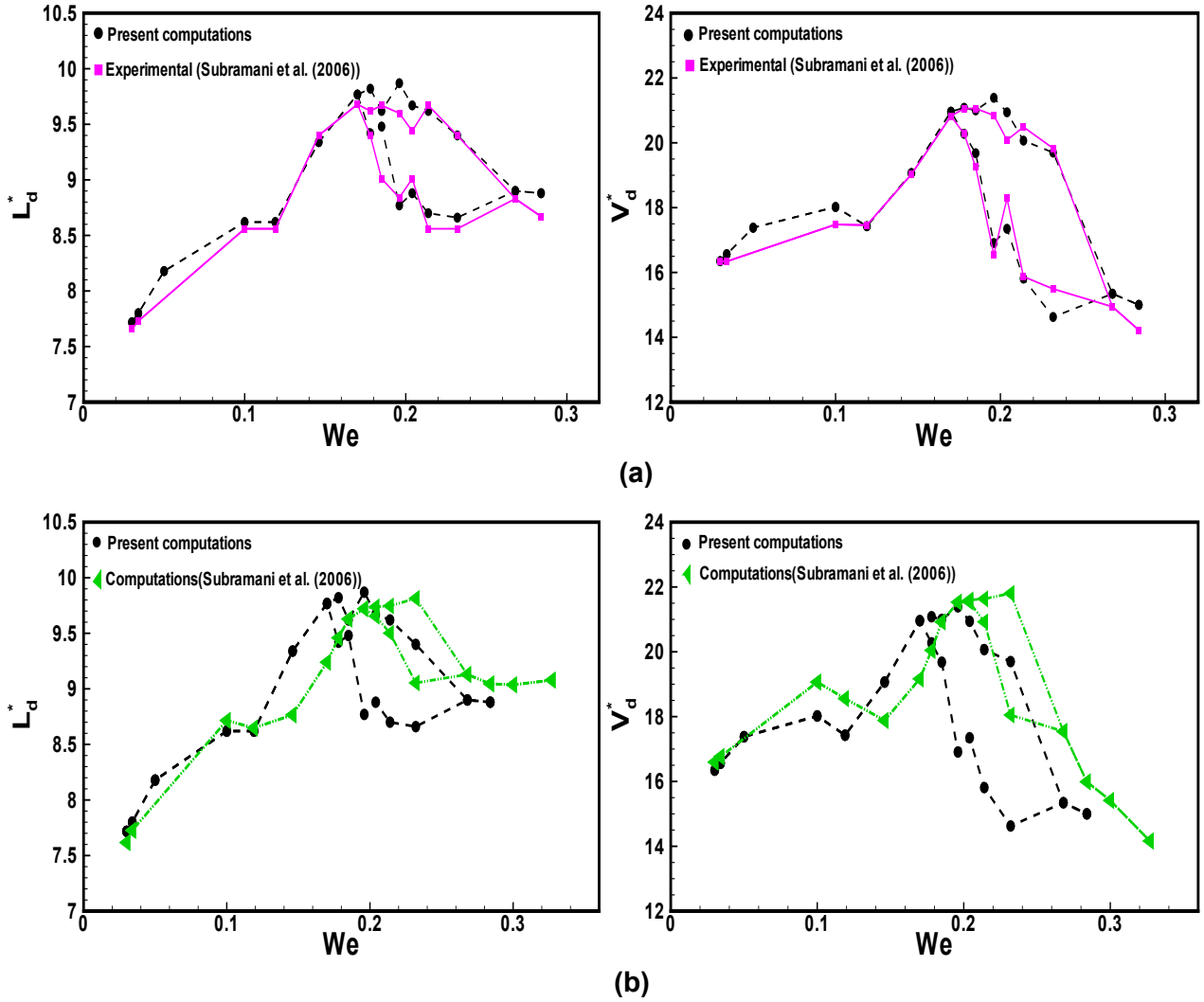

Fig. 9. Bifurcation diagram that shows comparison of computationally determined results with (a) experimentally results and (b) computation results based on 1D simulation of Subramani et al.(2006) for limiting length variation with We (left) and detached primary drop volume with We (right) under the conditions of $Oh = 0.13$, $Bo = 0.33$, $\eta = 8.961\times10^{-4}$ and $\lambda = 3.165\times10^{-4}$.

Transition Weber numbers	Experiment	Computation 1-D model	Present work
We_s	0.034	0.030	0.045
We_d	0.17	0.196	0.17
We_c	0.268	0.268	0.268
We_j	0.284	0.327	0.285

Table 3: Comparison between present results, and experiment and computation results based on 1-D model of Subramani et al.(2006) . Here, We_c is the critical Weber number which signals the transition from CD to P1. The pertinent input parameters are $Oh = 0.13$, $Bo = 0.33$, $\eta = 8.961\times10^{-4}$ and $\lambda = 3.165\times10^{-4}$.

3.4 Drop formation dynamics at high Bond number

The formation of drops at high Bond number has received little attention in literature. The dynamics of the dripping response, jetting response and the transition from dripping to jetting can be found in details in the literature (Ambravaneswaran et al., 2000; Ambravaneswaran et al., 2004; Subramani et al., 2006), but only for two different values of Bo=0.33 and 0.5. Furthermore, Subramani et al .(2006) reported numerical results of drop formation for $0.6 \le Bo \le 1.2$ when Oh=0.1 and We=0.05. Therefore, in this subsection, the new computation results are presented on the dynamics of drops formation by varying the Weber numbers in which the Bond number is kept high at Bo=2.205 and the Ohnesorge number is Oh=0.023. Figure 10 shows the time evolution of growing drop length in (a) P1S response when We=0.0133, (b) chaotic response when We=0.0146, (c) P2S response when We-0.0177 and (d) J response when We=0.02. Figure 11 also illustrates the time evolution of drop formation in (a) P2S response and (b) J response. It can be seen from the results of Figures 10 (c) and 11 (a) the existence of new dynamics P2S in the dripping regime which was not discussed earlier in the literature. It is observed that in P2S response the primary drops of two different limiting length $L_d^* = 5.6 \pm 0.1$ and $L_d^* = 4.1 \pm 0.1$ with satellite drop are formed successively. The time evolution illustrating L^* in Figure 10(d) shows

that when $t^* < 45$, drops are formed in dripping response. However, at $t^* = 45$ the growing drop length L^* undergoes an abrupt change and increases to a large value where the system exhibits J

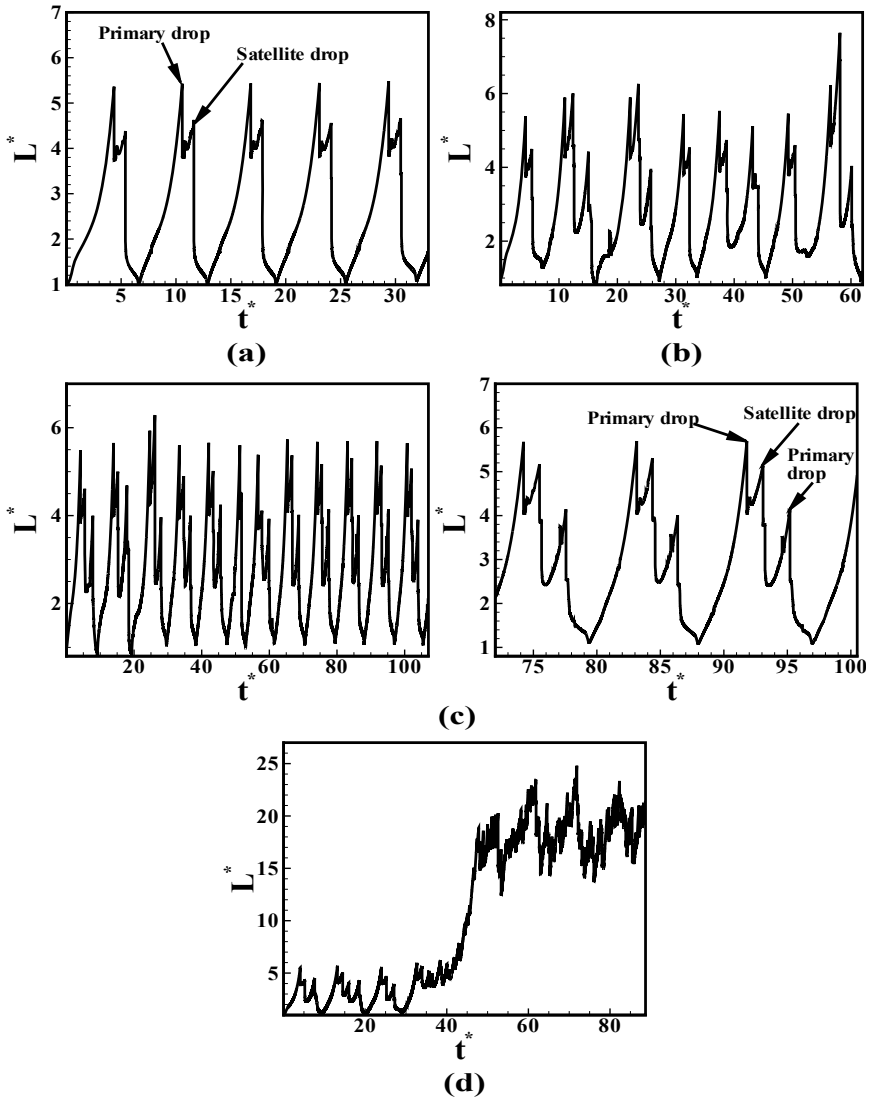

Fig. 10. Time evolution of growing drop length at each value of We when $Oh = 0.023$, $Bo = 2.205$, $\eta = 1.10\times10^{-3}$ and $\lambda = 2.20\times10^{-3}$: (a) P1S at $We = 0.0133$,(b) chaotic at $We = 0.0145$, (c) P2S at $We = 0.0177$ for $0 \le t^* \le 105$ (left) and $72 \le t^* < 101$ (right; zoom view of left part) (d) J at $We = 0.020$.

response. The results of Figure 10(d) that at $t^* > 50$ the column of liquid fluctuates with time and the average limiting length of the almost stable liquid jet is $L^*_{d,avg} \approx 20$ with minimum and maximum values of $L^*_{d,min} \approx 15$ and $L^*_{d,max} \approx 25$. This result is similar to that observed by Clanet

and Lasheras(1999), and numerically by Pan and Suga(2006), and Delteil et al. (2011). Most importantly, the result of Figure 10(d) also indicates that the system exhibits the transition from dripping to jetting and the transition occurs when We=0.02. The detailed analysis of the dynamics of the formation of drops including dripping, jetting, the transition from dripping to jetting and the hysteresis at high Bond numbers will be addressed experimentally and numerically further in our near future work.

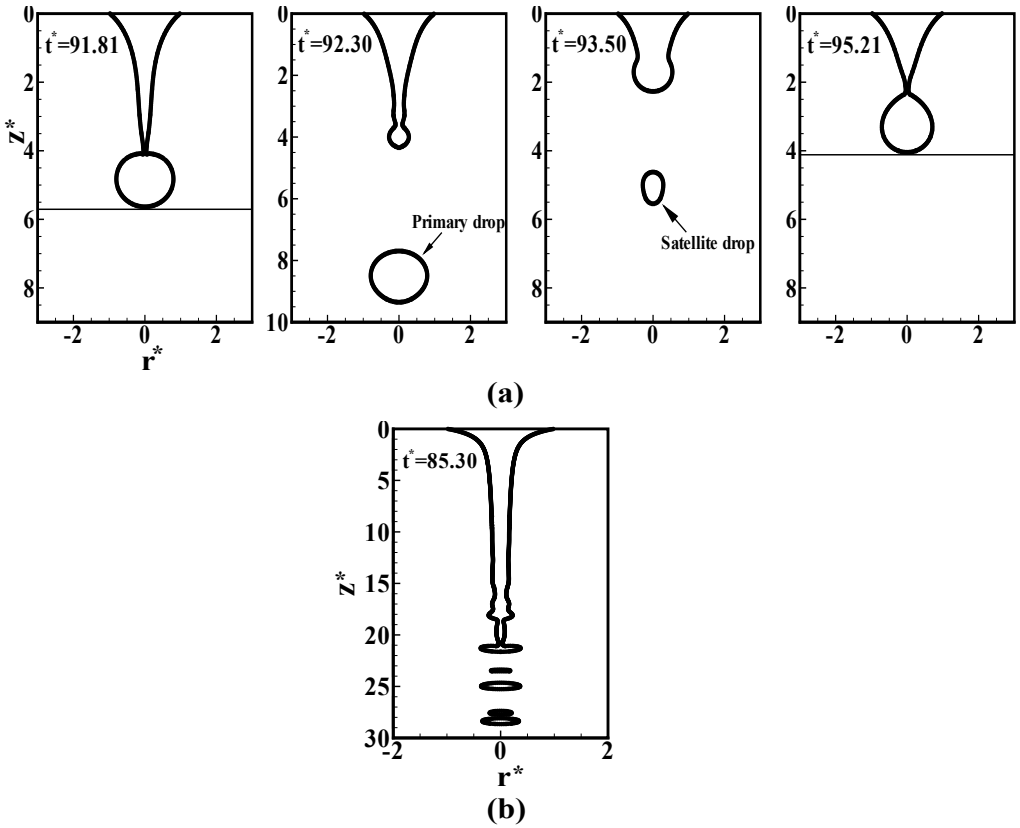

Fig. 11. (a) Time sequence of drop profiles in P2S response at $\mathrm{We} = 0.0177$, and (b) drop formation in J response at $\mathrm{We} = 0.020$. The pertinent input parameters are $\mathrm{Oh} = 0.023$, $\eta = 1.1\times10^{-3}$ and $\lambda = 2.20\times10^{-3}$.

Conclusions

We have presented a numerical study on the dynamics of the formation of drops into air using a CLSVOF method governed by axisymmetric Navier-Stokes equations. The numerical simulations have been carried out for a wide range of non-dimensional parameter Weber number, $1.8\times10^{-4} \le \mathrm{We} \le 7.0\times10^{-1}$ while keeping constant values of Oh = 0.01, 0.023 and 0.13, Bo = 0.33, 0.5 and 2.205, $\eta = 8.961\times10^{-4}$, 1.0×10^{-3} and 1.1×10^{-3}, and $\lambda = 3.165\times10^{-4}$, 2.20×10^{-3} and

7.1×10^{-3}. In this work, the rich dynamics of dripping response, jetting response and the transition of different responses were discussed. The present results are demonstrated after careful grid refinement investigations.

The present computations were focused to validate the predicted numerical results of the axisymmetric formation of drops with the experimental and 1D simulation results of Ambravaneswaran et al. (2004) and Subramani et al. (2006). The predicted results with respect to limiting length of drop at breakup and the volume of the detached primary drop show good agreement with the experimental results. It is observed that in the regime of nonlinear dynamics of drop formation, the predictions of the present computed results show much better accuracy than that of the 1D simulation results. Based on our numerical results, we can stress that the three dimensional but axisymmetric governing equations can be used to ensure good accuracy of the dynamics of drop formation for a wide range of dimensional parameters. Furthermore, our computation results reveal the existence of new dynamics period-2 with satellite drop (P2S) response which was not observed at low to moderately high Bond numbers before in literature.

Acknowledgments

The authors wish to acknowledge financial support from the Spanish MINECO under Project No. DPI2011-28356-C03-02.

References

Ambravaneswaran, B., Philips, S. D., Basaran, O. A., 2000. Theoretical analysis of a dripping faucet. Phys. Rev. Lett. 85, 5332-5335.

Ambravaneswaran, B., Wilkes, E. D., Basaran, O. A., 2002. Drop formation from a capillary tube: comparison of one-dimensional and two-dimensional analyses and occurrence of satellite drops. Phys. Fluids 14, 2606-2621.

Ambravaneswaran, B., Subramani, H. J., Philips, S. D., Basaran, O. A., 2004. Dripping-jetting transitions in a dripping faucet. Phys. Rev. Lett. 93, 0345011-0345014.

Basaran, O. A. 2002. Small-scale free surface flows with breakup: drop formation and emerging applications. AIChE. J. 48, 1842-1848.

Brackbill, J.U., Kothe, D.B., Zemach, C., 1992. A continuum method for modeling surface tension. J. Comput. Phys. 100, 335-354.

Chakraborty, I., Ray, B., Biswas, G., Durst, F., Sharma, A., Ghoshdastidar, P. S., 2009. Computational investigation on bubble detachment from submerged orifice in quiescent liquid under normal and reduced gravity. Phys. Fluids 21, 06210301-06210317.

Chakraborty, I., Biswas, G., Ghoshdastidar, P. S., 2011. Bubble generation in quiescent and co-flowing liquids. Int. J. Heat Mass Transfer 54, 4673-4688.

Chakraborty, I., Biswas, G., Ghoshdastidar, P. S., 2013. A coupled level-set and volume-of-fluid method for the buoyant rise of gas bubbles in liquids. Int. J. Heat Mass Transfer 58, 240-259.

Che, Z., Wong, T. N., Nguyen, N. T., Yap, Y. F., Chai, J. C., 2011. Numerical investigation of upstream pressure fluctuation during growth and breakup of pendant drops, Chem. Eng. Sci. 66, 5293-5300.

Chen, A. U., Notz, P. K., Basaran, O. A., 2002. Computational and experimental analysis of pinch-off and scaling. Phys. Rev. Lett. 88, 1745011-17450114.

Clanet, C., Lasheras, J. C., 1999. Transition from dripping to jetting. J. Fluid Mech. 383, 307-326.

Clift, R., Grace, J.R., Weber, M.E., 1978. Bubbles, Drops and Particles. Academic Press, New York.

Delteil, J., Vincent, S., Erriguible, A., Subra-Paternault, P., 2011. Numerical investigations in Rayleigh breakup of round liquid jets with VOF method, Comput. Fluids 50, 10-23.

Eggers, J., 1997. Nonlinear dynamics and breakup of free surface flows. Rev. Mod. Phys. 69, 865-929.

Eggers, J., Villermaux, E., 2008. Physics of liquid jets. Reports on Progress in Physics 71, 036601-0366079.

Eggers, J., Dupont, T. F. , 1994. Drop formation in a one-dimensional approximation of the Navier–Stokes equation. J. Fluid Mech. 262, 205-221.

Gueyffier, D., Li, J., Nadim, A., Scardovelli, R., Zaleski, S., 1999. Volume-of-fluid interface tracking with smoothed surface stress methods for three-dimensional flows. J. Comput. Phys. 52, 423-456.

Harlow, F. H., Welch, J.E., 1965. Numerical calculation of time-dependent viscous incompressible flow of fluid with free surface. Phys. Fluids 8, 2182-2189.

Heideger, W. Z., Wright, M. W., 1986. Liquid extraction during drop formation: Effect of formation time, AIChE. 32, 1372-1376.

Henderson, D. M., Pritchard, W. G., Smolka, L. B., 1997. On the pinch-off of a pendant drop of viscous fluid, Phys. Fluids 9, 3188-3200.

Hirt, C.W., Nichols, B.D., 1981. Volume of fluid (VOF) method for the dynamics of free boundaries. J. Comput. Phys. 39, 201-225.

Kumar, R., Kuloor, N.R., 1970. The formation of bubbles and drops. Chem. Eng. Sci. 8, 255-368.

Osher, S., Sethian, L.A., 1988. Fronts propagating with curvature-depending speed: algorithms based on Hamilton–Jacobi formulation. J. Comput. Phys. 79, 12-49.

Pan, Y. , Suga, K., 2006. A numerical study on the breakup process of laminar liquid jets into a gas. Phys. Fluids 18, 0521011-0521011.

Peregrine, D. H., Shoker, G., Symon, A., 1990. The bifurcation of liquid bridges. J. Fluid Mech. 212, 25-39.

Rayleigh, L., 1879. On the instability of jets. Proc. London Math. Soc. 10, 4.

Schulkes, R. M. S. M., 1994. The evolution and bifurcation of a pendant drop. J. Fluid Mech. 278, 83-100.

Shield, T. W., Bogy, D. B., Talke, F. E., 1987. Drop formation by DOD ink-jet nozzles: A comparison of experimental and numerical simulation. IBM J. Res. Dev. 31, 96-110.

Son, G., Hur, N., 2002. A coupled level-set and volume-of-fluid method for the buoyancy-driven motion of fluid particles. Num. Heat Transfer B 42, 523-542.

Subramani, H. J., Yeoh, H. K., Suryo, R., Xu, Q., Ambravaneswaran, B., Basaran, O. A. , 2006. Simplicity and complexity in a dripping faucet. Phys. Fluids 18, 03210613.

Sussman, M., Puckett, E.G., 2000. A coupled level set and volume-of-fluid method for computing 3D and axisymmetric incompressible two-phase flows. J. Comput. Phys. 162, 301-337.

Yildirim, O. E., Xu, Q., Basaran, O. A., 2005. Analysis of the drop weight method. Phys. Fluids 17, 0621071-06210713.

Wilkes, E. D., Philips, S. D., Basaran, O. A., 1999. Computational and experimental analysis of dynamics of drop formation. Phys. Fluids 11, 3577-3598.

Wilson, S. D. R., 1988. The slow dripping of a viscous fluid. J. Fluid Mech. 190, 561-570.

Zhang, X., Basaran, O. A., 1995. An experimental study of dynamics of drop formation. Phys. Fluids 7, 1184-1203.

Zhang, D. F., Stone, H. A., 1997. Drop formation in viscous flows at a vertical capillary tube. Phys. Fluids 9, 2234-2242.

Zhang, X., 1990. Dynamics of growth and breakup of viscous pendant drops into air, J. Colloid Sci. 212, 107-122.